Mon. Not. R. Astron. Soc. **319**, 484–496 (2000)

Radio circular polarization of active galaxies

D. P. Rayner,[1]★ R. P. Norris[2] and R. J. Sault[2]
[1]*School of Physics and Mathematics, University of Tasmania, GPO Box 252-21, Hobart, TAS 7001, Australia*
[2]*Australia Telescope National Facility, CSIRO, PO Box 76, Epping, NSW 2121, Australia*

Accepted 2000 July 12. Received 2000 June 19; in original form 1999 July 12

ABSTRACT

We present the first results of a circular polarization survey conducted with the Australia Telescope Compact Array (ATCA). We demonstrate the ability to make circular polarization measurements with a standard error of only 0.01 per cent, and have detections from both blazar and non-blazar active galactic nuclei (AGN). Our results show that, as a group, BL Lac sources and quasars have systematically higher circular polarization than radio galaxies. We demonstrate the association of high levels of circular polarization with total-intensity variability and flat/inverted spectral index as further evidence that circular polarization is associated with blazar activity. We also include preliminary circular polarization monitoring data and the detection of circular polarization from the GHz Peaked Spectrum (GPS) source PKS 1934–638, and discuss possible implications.

Key words: polarization – galaxies: active.

1 INTRODUCTION

1.1 Circular polarization of active galaxies

Circular polarization[1] has long been regarded as a potentially important tool for the study of extragalactic radio sources. Attempts to make use of it have generally been frustrated, however, because it is so difficult to measure. Analysis of the collation of circular polarization data presented by Weiler & De Pater (1983), generally from the 1970s, demonstrates the problem of circular polarization experiments; out of 50 radio galaxies and 43 quasars, circular polarization was detected at least twice at the 2.5σ level for only six radio galaxies and 15 quasars. For these detections, circular polarization levels are typically $m_c \sim 0.1$–0.2 per cent; lower levels would not have been detected. The only major circular polarization survey results published since are Komesaroff et al. (1984).

Despite the difficulties, a number of characteristics of circular polarization have been identified. There is an established correlation between flat-spectrum sources and high degrees of circular polarization (Conway et al. 1971; Roberts et al. 1975; Weiler & Wilson 1977); circular polarization is highly variable (Roberts et al. 1975; Seielstad & Berge 1975; Komesaroff et al. 1984), but there appears to be no correlation with linear polarization (Gilbert & Conway 1970; Roberts et al. 1975; Seielstad & Berge 1975).

★ E-mail: d_rayner@postoffice.utas.edu.au

[1] Circular polarization is given by the Stokes parameter V, which can be either +ve (*right-handed*) or −ve (*left-handed*) (IAU Transactions, 1974, XVB). It is often, however, the circularly polarized fraction $m_c = |V|/I$ (often expressed as m_c[per cent] $= 100 \times |V|/I$) of the total intensity Stokes I which is of interest.

1.2 Circular polarization emission mechanisms

A number of mechanisms have been put forward to explain the circular polarization detections in extragalactic radio sources. The first of these is synchrotron emission (so-called *intrinsic* circular polarization), for which the theory for transparent, homogeneous sources is given by Roberts & Komesaroff (1965) and extended by Legg & Westfold (1968). The fractional intrinsic circular polarization is derived as $m_c \sim 1/\gamma$, where γ is the Lorentz factor of electrons dominating the emission at the observed frequency ν. It follows from the synchrotron critical frequency $\omega_c \propto \gamma^2 B_o \sin\theta$ that the frequency dependence is (to first order) $m_c \propto \nu^{-1/2}$, where B_o is the magnetic field strength, and θ the angle between the magnetic field and the line of sight to the observer. The theory for intrinsic circular polarization from homogeneous self-absorbed emission regions is treated by Melrose (1971), who predicts a change in sign across the synchrotron self-absorption turnover.

Further theoretical studies suggested that circular polarization may be produced principally as a propagation effect. The most commonly proposed mechanism originates from the ellipticity of the characteristic modes of a relativistic plasma, and effects cyclic conversion of linear polarization to circular polarization, a mechanism physically similar to a quarter-wave plate. The process has been termed *circular repolarization* by Pacholczyk (1973). A succinct visualization of this mechanism is provided by Kennett & Melrose (1998), who explain the phenomenon in term of the rotation of the polarization vector on the Poincaré Sphere about the axis defined by the characteristic modes. The fractional circular polarization spectrum which arises through conversion is predicted to be steeper than that of intrinsic circular polarization; Pacholczyk (1973) predicts a circular polarization spectral index α_V, defined as $m_c \propto \nu^{+\alpha_V}$, of $\alpha_V \sim -1$, for a plasma with $\gamma > 2$,

but for which the propagation effects in the plasma are dominated by the properties of the 'cold' and low-power relativistic electrons. Melrose (1997) derives $\alpha_V \sim -3$ for a purely relativistic plasma.

A number of authors have attempted to determine the circular polarization emission mechanism by fitting the observed circular polarization spectrum with a power law, generally without success (Conway et al. 1971; Pacholczyk & Swihart 1974; Roberts et al. 1975). This is probably not surprising, given that a real source will be inhomogeneous, consisting of multiple components with different Lorentz factors and optical depths. Further, a detailed theoretical investigation of the spectral behaviour of circular polarization for a homogeneous plasma is given in Jones & O'Dell (1977), who note that in general both conversion and synchrotron emission contribute to the observed circular polarization; especially around the turnover frequency, the spectrum of fractional circular polarization is neither the $\alpha_V = -1$ predicted by conversion nor the $\alpha_V = -1/2$ expected for intrinsic synchrotron emission. Another possible circular polarization emission mechanism is provided by rotation measure inhomogeneities in an intervening plasma screen (Macquart & Melrose 1998).

1.3 Circular polarization variability

The very small fractions of circular polarization observed in extragalactic sources means that it is hard even to detect it, let alone measure circular polarization variability! A number of attempts have been made (Seaquist, Gregory & Clarke 1974; Ekers, Weiler & van der Hulst 1975; Roberts et al. 1975; Seielstad & Berge 1975; Ryle & Brodie 1981), but in most cases the circular polarization detections are less than 3σ, for most of the sources, for most of the time. Significant circular polarization results were obtained by Komesaroff et al. (1984), but no clear trend or correlation with total intensity or linear polarization was established. It was noted, however, than most sources have a *preferred handedness*, and that circular polarization varies more than total intensity or linear polarization.

The 'traditional' explanation for variability in blazar sources (Komesaroff et al. 1984) is an intrinsic mechanism, where flux variations are due to the ejection of new components from the core. Intrinsic explanations for polarization variations are possible even when the polarization variations appear unrelated to the total intensity variations. These models involve multiple, differently polarized components; such a situation is likely in blazar sources, as new components emerge from the core, and then expand and become optically thin.

Circular polarization arising as a propagation effect may also change as the properties of the plasma change; e.g., the magnetic field strength and plasma density decrease as a jet component expands. In sources where scintillation is important, this mechanism may also cause the circular polarization to be variable.

1.4 Circular polarization with the ATCA

The Australia Telescope Compact Array (ATCA) was designed from the outset to have the ability to make accurate measurements of circular polarization (Frater, Brooks & Whiteoak 1992). The feed-on-axis antenna design maintains high polarization purity, and the use of linearly polarized feeds largely isolates Stokes *V* from contamination by the much larger Stokes *I*. The linearly polarized feeds, coupled with the highly stable instrumental polarization, enable very accurate circular polarization measurements to be made with a comparatively small number of antennas.

We are using the ATCA to investigate a number of aspects of AGN circular polarization. In this paper we report the first results of an AGN circular polarization survey and monitoring campaign. The results of investigations of other properties of circular polarization, such as spectral dependence, will be the subject of a future paper.

1.5 Active galaxy nomenclature

The prevailing view of active galactic nuclei (AGN) (Urry & Padovani 1995) is that the gravitational potential energy of a central supermassive black hole supplies ionization energy for line emission, and also energetic particles which escape as collimated radio-jets with a wide variety of power.

This paper is concerned only with radio-loud AGN – indeed, extremely radio-loud AGN. For our purposes, it is generally sufficient to divide sources into three optical classes:

BL Lac objects, which have compact cores characterized by a lack of strong emission lines (Stickel, Fried & Kühr 1993).

Quasars, whose optical continuum is dominated by a bright core and spectral profile by broad emission lines. The quasars discussed in this paper all have a flat radio spectrum and a core-dominated radio morphology, and all correspond to the Flat Spectrum Radio Quasar (FSRQ) definition of Urry & Padovani (1995). BL Lac and FSRQ objects are sometimes referred to collectively as *blazar* objects.

Galaxies, in which the optical morphology is not dominated by a bright core. Radio-loud galaxies can be further usefully subdivided according to the radio morphology and spectra:

(i) Fanaroff–Riley class I and class II (**FR I** and **FRII**) galaxies (Fanaroff & Riley 1974) are characterized by extensive radio structure on kpc–Mpc scales, which may extend well beyond the extent of the host galaxy.

(ii) In Compact Steep Spectrum (**CSS**) galaxies, the radio emission is contained within the host galaxy ($\lesssim$15 kpc), and the radio spectrum characterized by a steep power law turning over near 100 MHz (O'Dea 1998).

(iii) The radio emission in GHz Peaked Spectrum (**GPS**) galaxies is contained within the narrow-line region of the AGN ($\lesssim$1 kpc), and generally has a spectral turnover at $\gtrsim$1 GHz (O'Dea 1998).

2 SOURCE SELECTION PROCEDURE

There has been no circular polarization survey of a well-defined sample of extragalactic sources, so the selection effects in published data are largely unknown. Further, the low signal-to-noise ratios of most circular polarization experiments have resulted in an interpretation of the circular polarization phenomena based mainly on sources with 'strong' circular polarization. We have defined a new sample of AGN on which to conduct a high-precision search for circular polarization.

Ideally, we would have liked to select sources at a low radio-frequency. Low-frequency emission is dominated by synchrotron emission from optically thin, extended components, whereas high-frequency emission is increasingly dominated by beamed synchrotron emission from AGN jets. Doppler boosting (Blandford & Königl 1979) will induce an orientation bias in samples chosen at frequencies where beamed emission is significant; the sources chosen will have jets directed preferentially towards the observer.

A sample selected at a low frequency avoids any such bias, but such a selection would, however, have presented several problems. First, the sample would have been dominated by sources in which compact components are weak or absent, and we expect that our sensitivity would be inadequate to detect circular polarization from such sources. Secondly, there would be too few BL Lac type sources in the sample to allow their inclusion in any statistical analysis of the results, and the circular polarization properties of these sources are of significant interest (Ekers et al. 1975). Finally, for circular polarization observations with the ATCA, highly extended sources pose a substantially more difficult calibration problem than compact sources.

Our sample is a compromise. It effectively consists of three samples: the first of BL Lacs, the second of radio galaxies and quasars, and the third of miscellaneous sources.

Our sample was initially selected from the Parkes-MIT-NRAO (PMN) catalogues (Griffith 1992). These catalogues, observed at 4.85 GHz, are virtually complete for strong, compact sources. We recognize that selection on 4.85-GHz flux means that we have an orientation-bias in our sample. We began the selection process by taking the PMN survey, and adding the following constraints.

(i) Sources with $S_{4.85\,\mathrm{GHz}} > 1$ Jy were selected. Assuming no instrumental artefacts or dynamic-range limitations, a 1 Jy beam^{-1} source is about the weakest source for which the ATCA can detect $m_c \sim 0.01$ per cent, at the 3σ level, in 12 hours, at 4.8 GHz.

(ii) Sources with $Dec_{2000} > -20°$ were excluded. This gives a good parallactic-angle coverage for polarization calibration (ATCA is at latitude of $-30°$), and limits visibility-degradation at low elevation.

(iii) Sources were excluded if they have galactic latitude $|b| < 20°$. Known galactic objects were also removed from the sample.

(iv) Sources within $6\overset{\circ}{.}5$ of the centre of the LMC and within 2° of the centre of the SMC were excluded.

This process yields a sample of 131 objects, for which optical identifications were taken from the NASA/IPAC Extragalactic Data base (NED). The first sources selected for our sample were the eight sources in the 131 sample listed as BL Lac objects in NED.

For the second sample, the radio galaxies and quasars, two additional constraints were applied to the remaining 123 sources:

(i) include only sources with $Dec_{2000} < -60°$, and

(ii) include only sources which have a peak flux density $S_{4.8\,\mathrm{GHz}} > 800$ mJy when observed at resolutions comparable to the ATCA.

The first constraint serves to reduce the size of the sample in a well-defined way, and also to eliminate any calibration problems which might result from sources passing close to the zenith, as described in Rayner et al. (in preparation).

The second constraint eliminates those extended sources for which the peak flux density is too low for us to achieve our target sensitivity. Setting the flux threshold at 800 mJy means that sources are less likely to be excluded on account of variability. ATCA data were available for all sources; especially useful were the data base generated by Prouton (in preparation) from Wright et al. (1997), and also the ATCA Calibrator Source Catalogue (Duncan & Sproats 1992; Lovell 1996; Reynolds 1997). The radio galaxies PMNJ 2157–6941 and PMNJ 2356–612 were excluded to avoid calibration problems which may arise due to the complex extended structure of these sources (Koekemoer 1996; Fosbury et al. 1998).

In addition to the sources specifically selected for the survey, a number of other sources have been observed for circular polarization by way of instrumental tests and feasibility studies. These make up the third component of our sample. These extra sources have not been selected or observed in a consistent manner. Their properties are not, however, expected to vary significantly from those selected from the PMN catalogues. One possible difference is that the extra sources are all point sources, as they were selected to be used as calibrators, whereas some of the sources selected from the PMN catalogues contain multiple components.

The source sample is listed in Table 1. The 'selection criteria' column indicates whether a source was observed because (a) it was included in the 131-source sample, and was listed as a BL Lac in NED, (b) it was included in the 131-source sample, and had $Dec_{2000} < -60°$, or (c) it was a miscellaneous source.

The identifications given by NED have been checked with other listed citations, and corrected where appropriate – references are given in Table 1. Our definition of a BL Lac object is that given by Stickel et al. (1993). Even with a clear definition for a BL Lac, however, the classification of a blazar object can still be somewhat arbitrary, depending as it does on the state of the source when observed. Sources for which the spectroscopic data are ambiguous are marked with a '?' in Table 1.

We note that our BL Lac sample may not be complete for the region and flux cut-off specified, as there may be BL Lac objects misidentified in NED. In particular, a number of sources have no spectroscopic identification, and have been classified as quasars based on optical morphology; these sources are marked with a '‡' in the 'ID' column in Table 1.

3 OBSERVATION AND CALIBRATION

A detailed description of the observational requirements and calibration procedures for circular polarization observations with the ATCA are given by Rayner et al. (in preparation). Here we briefly describe the specifications of the ATCA, and mention some of the important concepts and procedures associated with circular polarization observation and data processing.

3.1 Observational procedure

ATCA consists of six 22-m alt-azimuth antennas near Narrabri, New South Wales (Frater et al. 1992). Each ATCA antenna is equipped with two wide-band feeds, and the appropriate feed for the requested frequency is automatically placed at the focus. In addition, two separate frequencies can be observed with each feed at the same time. The observations detailed here were made simultaneously at 4.800 and 4.928 GHz in the ATCA 'continuum-mode', which gives 32 (partially overlapping) channels covering a bandwidth of 128 MHz at each frequency.

Sources were typically observed for 1–12 hours each, spread over an hour-angle range of close to 12 hours. For such synthesis observations, the ATCA has a resolution of ~2 arcsec. The phase centre was offset from the antenna pointing centre by 10 or 20 arcsec to isolate any phase-centre artefacts. No hardware modifications are required for circular polarization measurements.

The GPS source PKS 1934–638 was used as the primary flux calibrator. The total-intensity spectrum and linear polarization are known (Reynolds 1994), while a discussion on the level of circular polarization assumed for PKS 1934–638 is given below.

Table 1. Source sample for the circular polarization survey. The 'selection criteria' are (a) listed as a BL Lac in NED, (b) had $Dec_{2000} < -60°$, or (c) was a miscellaneous source.

PMN Name	b1950 Name	PMN Flux (Jy)	selection criteria	ID	z	Optical Refs
0229–7847	0230–790	0.5	c	QSO	1.097	5,17
0252–7104	0252–712	1.7	b	G (CSS)	0.563	2,29
0303–6211	0302–623	1.9	b	QSO‡	–	31
0309–6058	0308–611	1.1	b	QSO‡	–	5
0406–3826	0405–385	0.8	c	QSO	1.285	21,23,30
0408–6545	0407–658	3.6	b	G (CSS)	–	2,24
0408–7507	0409–752	4.6	b	G (FRII)	0.694	1,22
0428–3756	0426–380	1.2	a	BLC	>1.03	26
0440–4332	0438–436	3.9	c	QSO	2.852	19
0450–8100	0454–810	1.4	b	QSO	0.444	12,25
0453–2807	0451–282	2.2	c	QSO	2.559	34
0457–2324	0454–234	1.9	a	BLC?	1.009	12,25,32
0506–6109	0506–612	1.2	b	QSO	1.089	16,33,35
0538–4405	0537–441	4.8	a	BLC	0.896	12,26
0635–7516	0637–752	6.4	b	QSO	0.651	12,14,29,33
0743–6726	0743–673	2.2	b	QSO	1.512	2,4,7,13
1018–3144	1015–314	1.8	c	G? (CSS)	1.346	2
1037–2934	1034–293	1.5	a	QSO?	0.312	6,15,25,33
1147–3812	1144–379	1.8	a	BLC	1.048	25,26
1517–2422	1514–241	2.0	c	BLC	0.048	18,26,28,29
1522–2730	1519–273	1.8	a	BLC	≳0.2	12,26
1819–6345	1814–637	4.5	b	G (CSS)	0.063	29
1835–7150	1829–718	1.1	b	no ID	–	27
1837–7108	1831–711	2.3	b	QSO	1.356	12,16
1912–8010	1903–802	1.3	b	QSO	∼0.5	3,12
1930–6056	1925–610	0.9	c	QSO‡	–	17
1939–6342	1934–638	5.9	b	G (GPS)	0.183	11
1940–6908	1935–692	1.0	b	QSO	3.154	16,20
2009–4849	2005–489	1.2	a	BLC	0.071	8,9,26,32
2152–7807	2146–783	1.1	b	QSO‡ (GPS)	–	17
2243–2544	2240–260	1.2	a	BLC	0.774	26

Notes for Table 1: ‡ no spectroscopic identification available; ? spectroscopic classification uncertain.

References to Table 1: (1) Alvarez et al. (1993); (2) di Serego Alighieri et al. (1994); (3) Anguita et al. (1979); (4) Bergeron & Kunth (1984); (5) Bolton & Savage (1977); (6) Cristiani & Koehler (1987); (7) Espey et al. (1989); (8) Falomo et al. (1987); (9) Falomo, Scarpa & Bersanelli (1994); (10) Falomo (1996); (11) Fosbury et al. (1987); (12) Hewitt & Burbidge (1993); (13) Hunstead et al. (1971); (14) Hunstead, Murdoch & Shobbrook (1978); (15) Jauncey et al. (1978); (16) Jauncey et al. (1984); (17) Jauncey et al. (1989); (18) Morris & Ward (1998); (19) Morton, Savage & Bolton (1978); (20) Osmer, Porter & Green (1994); (21) Peterson & Bolton (1972); (22) Reynolds et al. (1993); (23) Savage & Wright (1981); (24) Stickel & Kühr (1996); (25) Stickel, Fried & Kühr (1989); (26) Stickel et al. (1993); (27) Stickel, Meisenheimer & Kühr (1994); (28) Strittmatter et al. (1972); (29) Tadhunter et al. (1993); (30) Véron et al. (1990); (31) Wall & Cannon (1973); (32) Wall et al. (1986); (33) Wilkes et al. (1983); (34) Wilkes (1986); (35) Wright et al. (1997).

Phase-reference calibrators were selected from the ATCA Calibrator Source Catalogue (Reynolds 1997).

3.2 Calibration

The 4.800- and 4.928-GHz observations were calibrated independently, which is standard practice for ATCA data. This is important, as the leakage parameters are expected to be band-dependent. The ATCA receivers are equipped with a noise-diode which injects a signal to allow continuous measurement of the phase-difference between the orthogonal feeds (*xy*-phase); this phase correction was applied before calibration. A residual *xy*-phase term is solved for in the calibration process; such a residual term may result, for example, if the noise-diode is slightly asymmetrical with respect to the two feeds. The residual *xy*-phase was assumed to be time-independent during calibration; tests showed this assumption to be justified (see below).

Calibration was done with the MIRIAD package (Sault, Teuben & Wright 1995). First, the bandpass was determined from the primary flux calibrator; the bandpass is assumed to be time-independent, and is applied to all the target and calibrator sources. This step also sets the zero-point for circular polarization. The main calibration step involves simultaneously solving for time-dependent complex-gains, time-independent residual *xy*-phase, and time-independent leakages for each feed, as well as the linear and circular polarization of the source. A good parallactic-angle coverage is required in order that the leakages and source linear polarization can be decoupled in the solution process through the relative rotation of the feeds and parallactic angle. The parallactic angle was determined individually for each antenna, using the antenna orientation determined from the pointing survey which is conducted after each ATCA reconfiguration.

Traditional polarization calibration of ATCA data assumes the 'weakly polarized' case (Sault, Killeen & Kesteven 1991), where terms in $leakage \times (Q, U)$ are neglected. When attempting to measure fractions of a per cent of circular polarization, these

second-order leakages are important. The MIRIAD calibration routines allow solution using the 'strongly polarized' matrix, which also solves for the second-order terms. To determine the coefficients in such a solution requires a source which has a few per cent linear polarization, so that there is sufficient signal in the second-order terms. If the target source itself did not have sufficient linear polarization to solve for these terms, or if it was significantly resolved, an unresolved and highly linearly polarized 'leakage calibrator' was used instead. The only term not determined from this calibration process is the alignment of the X-feed on the reference antenna, which can only be determined from observations of a source with accurately known linear polarization (Komesaroff et al. 1984). This leads to a small uncertainty in the linear-polarization position angle, which is of no consequence to this survey.

It is important to note that, with the orthogonal-linear feed arrangement on the ATCA, the circular polarization is essentially given by the difference in the cross-handed correlations on each baseline. Consequently, gain errors lead only to leakage of Stokes Q and U into V, whereas errors in the leakage terms result in corruption of V by I. This contrasts to the situation for arrays with approximately circularly polarized feeds, in which the circular polarization is given by the difference in the same-handed correlations, and gain errors cause leakage of the much larger I into V. Thus, for the linearly polarized feed design, it is the determination of the leakage terms, rather than the gains, which is critical. The leakage terms for the ATCA antennas are highly stable and can be determined very precisely (unlike the gains), giving the ATCA excellent circular polarization capabilities.

3.3 Circular polarization error budget

A detailed discussion of the error expected in an ATCA circular polarization observation is given in Rayner et al. (in preparation), but is discussed briefly here. The error formulation includes both the theoretical error and an empirically derived estimate of the systematic errors.

The fractional error in the measured circular polarization is taken to be

$$\sigma_{V/I}^2 = \sigma_{\rm t}^2 + \sigma_{\rm c}^2 + \sigma_{\rm z}^2 + \sigma_{\delta-+}^2 + \sigma_{\delta--}^2 + \sigma_{\gamma--}^2 \quad (1)$$

where terms on the right-hand side are defined as follows.

(1) σ_t is given by

$$\sigma_t = \left.\frac{rms}{I}\right|_{\rm target} \quad (2)$$

where *rms* is the rms of the Stokes V clean-residual image in a small region about the target source, and I is the peak flux-density of the target source. The term incorporates contributions from both system-noise and any residual non-physical artefacts.

(2) $\sigma_{\rm c}$ is given by

$$\sigma_{\rm c} = \left.\frac{rms}{I}\right|_{\rm primary} \quad (3)$$

where *rms* is the rms of the Stokes V image of the ATCA primary calibrator PKS 1934–638, and I is the flux density of PKS 1934–638. This term represents the precision with which the zero-point has been measured for a particular observation. The measured $\sigma_{\rm c}$ is usually close to what would be expected from system noise alone.

(3) σ_z is the error in the absolute zero-point of circular polarization, defined from circular polarization observations of CSS sources (see below) to be $\sigma_z = 0.005$.

(4) $\sigma_{\delta-+}$ is the error contribution from leakage of Stokes $I \rightarrow$ Stokes V. The error is empirically derived, from a comparison of the leakage terms for multiple calibration solutions, to be $\sigma_{\delta-+} \leq 2 \times 10^{-5}$, and depends in detail on the calibration path.

(5) $\sigma_{\delta--}$ and $\sigma_{\gamma--}$ are the expected level of error caused by leakage of linear polarization $\rightarrow$ circular. By definition, $\sigma_{\delta--}$ and $\sigma_{\gamma--}$ do not cause artefacts in the Stokes V clean-residual image; such artefacts are included in σ_t. These error terms were estimated from the comparison of the leakage ($\sigma_{\delta--}$) and xy-phase ($\sigma_{\gamma--}$) terms for multiple calibration solutions. These errors depend strongly on the source linear polarization, linear-polarization position angle, and declination. They were calculated individually for each source; the maximum error expected is $\sqrt{\sigma_{\delta--}^2 + \sigma_{\gamma--}^2} < 1 \times 10^{-4}$.

3.4 Consistency checks

A number of consistency checks have been made to verify the authenticity of the circular polarization measurements, both using measurements of the instrumental parameters and the circular polarization measurements themselves. Some of these tests are described briefly below.

The variations of the antenna leakage terms during a synthesis have been estimated using repeated observations of the ATCA primary calibrator PKS 1934–638. The principal source of variations in the antenna leakage terms was expected to be the rotation of the feed-horn mounting 'turret' (Frater et al. 1992) due to elevation-dependent gravitational torque. No leakage variations consistent with such rotations were observed. Peak rotations in one antenna of $\sim 2 \times 10^{-4}$ rad, of unknown origin, did not result in an observable error in the measured circular polarization ($\Delta V/I < 10^{-5}$). Similarly, no elevation-dependent variation in the measured circular polarization of PKS 1934–638 was observed, with the upper limit for elevation-dependent errors estimated to be $\Delta V/I < 2 \times 10^{-5}$.

A similar set of measurements determined that the xy-phase variability (after correction for the noise-diode measured xy-phase) had an rms of only 0°.02. This suggests that instrumental xy-phase variations have a negligible effect on the measured circular polarization ($\Delta V/I \lesssim 10^{-6}$).

Instrumental and calibration errors may leave non-physical looking artefacts in the Stokes V images. In particular, non-closing baseline-dependent errors or short time-scale variations in instrumental leakages are known to leave artefacts. Such artefacts will increase the rms in the Stokes V residual images over what would be expected due to system noise alone. The measured rms for the observations was compared with a theoretical estimate of the rms derived from the system temperature. This demonstrated that the circular polarization images were not significantly affected by artefacts, down to a limiting sensitivity of $V \lesssim 30\,\mu$Jy, implying $\Delta V/I \lesssim 3 \times 10^{-5}$ for a 1-Jy source.

As noted above, observations were made simultaneously in two adjacent bands at 4.800 and 4.928 GHz. Although both bands use the same feeds and front-end low-noise amplifiers, the two bands are calibrated independently in MIRIAD. The instrumental leakages are known to be significantly variable over even a single 104-MHz band (for 6-cm observations), so it is expected that the leakages for the two bands will be somewhat independent. Thus, comparison of the circular polarization results for two adjacent

bands provides a potentially useful consistency check. A comparison using the results from 45 independent observations demonstrated that the differences in the circular polarization results for the two bands were consistent with, and not more than 1.5 times, the differences expected from system noise alone.

Finally, the effect of the primary-beam polarization response of the ATCA antennas on the measured circular polarization has not been thoroughly investigated, but it is expected to be negligible for 6-cm observations near the pointing centre (Kesteven 1995). In addition, all the survey sources are dominated by compact structure, further limiting the possibility of primary-beam-related errors.

3.5 Imaging and flux measurement

The survey sources were usually dominated by a single, strong, unresolved component. This is partly because the lack of short baselines in the array configurations we used meant that our observations were insensitive to significantly extended emission. Once they were calibrated, the visibility data sets were Fourier-transformed, and then images of each Stokes parameter were cleaned individually. Antenna-based phase and/or amplitude self-calibration was applied using the clean model, if necessary, to improve the total-intensity and linear polarization images – such gain calibration made virtually no difference to the circular polarization images, as expected for an orthogonal-linear feed arrangement. As the images were dominated by point sources, and had been self-calibrated, the flux value for each Stokes parameter was simply taken as the flux value of the pixel at the nominal source position.

The 'full-polarization' image of PMNJ 0743–6726 – the most highly resolved source in the survey – is shown in Fig. 1. Contours show Stokes *I*, grey-scale Stokes *V*, and vectors represent the magnitude and direction of the linear polarization. The image has been corrected for the error in the circular polarization zero-point (see below). The array phase-centre is 20 arcsec north of the core position.

In total intensity, the source shows a 1.2-Jy, unresolved core as well as significant lobe emission with a peak flux density of ~310 mJy. All components are highly linearly polarized (core ~8 per cent, lobes up to 25 per cent). The circular polarization is associated with the core component only. The core has $V/I = 0.154$ per cent, and the rms of the image is only $\sigma_t = 0.004$ per cent. If the lobes were circularly polarized at the same level as the core, *then the lobes would be 9σ above the rms*. This image gives a very clear demonstration that circular polarization detections with the ATCA are not due to leakage of total intensity or linear polarization, as either case would lead to circular polarization being detected in the lobes.

3.6 Zero-point calibration

Unlike source linear polarization, which can be disentangled from instrumental leakages through differential parallactic-angle rotation, the zero-level for circular polarization must be fixed from observations of a source with 'known' polarization, in a manner similar to total intensity calibration. There are, however, no sources with circular polarization determined at the precision levels possible with the ATCA. Initially, the ATCA primary calibrator PKS 1934–638 was assumed to be circularly unpolarized. Were this assumption invalid, *all observations would be biased with a fractional circular polarization of equal magnitude and opposite handedness to that of PKS 1934–638.*

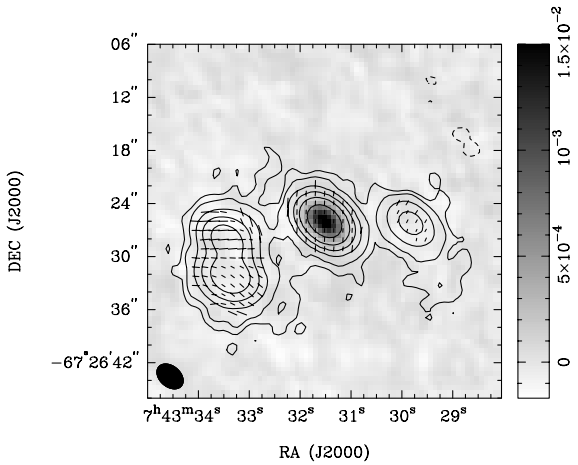

Figure 1. Full polarization, 6-cm image of PMNJ 0743–6726. Grey-scale shows Stokes *V* in Jy beam^{-1}. Contours show Stokes *I*; levels are −0.1 per cent, 0.2 per cent, 0.33 per cent, 1.0 per cent, 3.3 per cent, 10 per cent, 33 per cent and 99 per cent of $I_{\rm max} = 1.16$ Jy beam^{-1}. Vectors show linear polarization position angle and per centage, with the peak $m_{\rm l} =$ 25.2 per cent.

Table 2. Circular polarization of steep-spectrum sources.

b1950 Name	$S_{4.8\,\rm GHz}$ (Jy)	V/I ($\times 10^{-4}$)	σ_V/I ($\times 10^{-4}$)
0252–712	1.67	−2.01	0.3
0409–752 SE	2.43	−2.6	0.55
0409–752 NE	1.68	−3.5	0.75
1748–253	0.48	−1.5	2.1
1814–637	4.51	−3.06	0.15
2203–188	4.13	−4.1	0.4
2135–209	1.42	−3.2	0.7

Circular polarization calculated assuming $V = 0$ for the primary calibrator PKS 1934–638. The results are consistent with $V/I \sim 2.5 \times 10^{-4} \pm 0.5 \times 10^{-4}$ for PKS 1934–638.

Our survey results showed that steep-spectrum sources do not show high levels of circular polarization, so these sources provide a good check on the circular polarization of PKS 1934–638. The results of observations of steep-spectrum sources, from the survey and otherwise, are shown in Table 2. Were all steep-spectrum sources to have intrinsic circular polarization, and PKS 1934–638 to be unpolarized, we would expect *equal numbers to be left- and right-handed.* This is clearly not the case in Table 2. The apparent bias in the results suggest that PKS 1934–638 is, in fact, positively circularly polarized, with $V/I \sim (+2.5 \pm 0.5) \times 10^{-4}$. This is consistent with the results of Komesaroff et al. (1984), who found $V/I = +0.03 \pm 0.03$ per cent for observations around 5750 MHz.

Following the discovery of circular polarization in PKS 1934–638, an experiment to determine the circular polarization spectrum of PKS 1934–638 was conducted using observations of CSS sources (Rayner et al., in preparation). Theoretically, the low turnover frequency of CSS sources is expected to preclude linear to circular conversion, so these sources are ideal for setting the circular polarization zero-level. Observationally, no circular polarization has been detected from CSS sources at 6 cm with the ATCA. All the results quoted in this paper use the CSS-determined value of $V/I = (+2.9 \pm 0.5) \times 10^{-4}$ for PKS 1934–638.

Finally, we note that the level of circular polarization inferred for PKS 1934–638 is much smaller than the levels detected in the blazars in our survey, and the statistical tests detailed below were found to be insensitive to a small change in the zero-point. Thus a small error in the zero-point would not seriously affect the results in this paper.

3.7 Total intensity monitoring data

A programme of regular flux monitoring of compact, variable sources is currently being undertaken with the ATCA (Tornikoski et al. 1999). The observations nominally consist of 1–2 minutes of tracking for each of the four ATCA frequency bands, for each source. The data available for analysis were observed between 1996 July 27 and 1998 February 15, and consist of $z_i \pm \Delta z_i$ for each observing session, where:

z_i is the amplitude-averaged flux of the source in an observing session, and

Δz_i is the rms amplitude-scatter in the visibilities for that source over the session.

The data were used to generate variability and spectral-index statistics for the sources in our survey. A first attempt to characterize the variability was to use the 4800-MHz flux data to calculate the Fluctuation Index (Romerno, Benaglia & Combi 1995):

$$FI = \frac{\sigma}{\bar{z}}, \tag{4}$$

where $\bar{z}$ is the weighted-mean flux over all sessions, and σ is the standard deviation of all z_i.

It was found, however, that with a small number of epochs *FI* was dominated by flux measurements with large errors. Instead, we define the Weighted Fluctuation Index (*WFI*) as

$$WFI = \frac{\sigma_{\rm w}}{\bar{z}}, \tag{5}$$

where $\sigma_{\rm w}$ is the 'weighted standard deviation', given by

$$\sigma_{\rm w} = \frac{\sum_{i=1}^{n}\left[\left(\frac{1}{\Delta z_i}\right)^2 (z_i - \bar{z})^2\right]}{\sum_{i=1}^{n}\left(\frac{1}{\Delta z_i}\right)^2}. \tag{6}$$

Using $\sigma_{\rm w}$ reduced the contribution from points with large errors, and gave a much better characterization of the actual flux variability. A simple estimate of the uncertainty in the *WFI* was obtained by evaluating *WFI* n times, each time leaving out z_i, and taking the standard deviation of the resulting distribution as the error in *WFI*. The results are given in Table 3.

Just how useful is *WFI* as an indicator of variability is open to question. Given the fairly long time-scale of variability seen in most of the AGN in the survey, the monitoring data available may inadequately sample the activity cycle in some sources. Conversely, if circular polarization is associated with sources when they are in an active state, then the data available are appropriate. The biggest advantages of the ATCA monitoring data are that

Table 3. Survey results, including total intensity, linear polarization, circular polarization, spectral index and *WFI*. Circular polarization detections at the 5σ level are in bold.

PMN Name (J2000)	PKS Name (b1950)	ID	$I_{4.8\,\rm GHz}$ (Jy)	*LP* (per cent)	*V/I* (per cent)	$\sigma_{V/I}$ (per cent)	α_{3-20cm} ($I \propto \nu^{+\alpha}$)	$\sigma_{\alpha_{3-20cm}}$	*WFI* (per cent)	σ_{WFI} (per cent)
0229–7847	0230–790	QSO	0.6	0.6	**+0.45**	0.03	+0.5	0.1	6	2
0252–7104	0252–712	G (CSS)	1.7	0.0	+0.009	0.008	−1.2	*	1	★
0303–6211	0302–623	QSO	2.2	1.6	−0.003	0.009	−0.08	0.02	1.4	0.2
0309–6058	0308–611	QSO	1.3	2.1	−0.050	0.011	−0.15	0.1	3.1	0.3
0406–3826	0405–385	QSO	2.0	0.8	**−0.101**	0.009	+0.50	0.02	11	1
0408–6545	0407–658	G (CSS)	3.3	0.0	+0.020	0.008	−1.3	*	1	★
0408–7507 (NW)	0409–752	G (FRII)	1.8	4.3	−0.006	0.018	−1.1	*	1	★
0408–7507 (SE)	0409–752	G (FRII)	2.6	0.8	+0.003	0.009	−1.1	*	1	★
0428–3756	0426–380	BLC	1.6	3.4	**−0.109**	0.008	+0.11	0.03	20	1
0440–4332	0438–436	QSO	2.8	0.9	−0.023	0.009	−0.28	0.02	2.8	0.2
0450–8100	0454–810	QSO	1.0	1.5	**+0.142**	0.009	+0.12	0.02	5	2
0453–2807	0451–282	QSO	1.8	4.9	+0.016	0.018	−0.28	0.02	3.4	0.2
0457–2324	0454–234	BLC	1.7	1.0	**+0.263**	0.008	+0.4	0.1	12.3	0.5
0506–6109	0506–612	QSO	1.4	1.4	**−0.118**	0.008	−0.2	*	–	–
0538–4405	0537–441	BLC	3.8	0.9	**−0.065**	0.008	0.0	0.1	27	2
0635–7516	0637–752	QSO	6.1	0.8	+0.008	0.009	+0.2	*	2.6	0.2
0743–6726	0743–673	QSO	1.2	8.5	**+0.158**	0.011	–	–	–	–
1018–3144	1015–314	G (CSS)	1.4	0.0	+0.009	0.009	−0.79	*	1	★
1037–2934	1034–293	QSO	1.6	2.5	**+0.169**	0.009	+0.3	0.2	18	2
1147–3812	1144–379	BLC	1.2–1.5	2.3–2.7	**+0.139**	0.011	+0.1	0.2	22	2
1517–2422	1514–241	BLC	2.5	4.6	−0.046	0.010	+0.14	0.02	11	1
1522–2730	1519–273	BLC	1.44–1.60	0.2–3.0	**−0.25**–**−0.42**	0.02	+0.21	0.03	13	1
1819–6345	1814–637	G (CSS)	4.5	0.0	−0.002	0.007	−1.1	*	1	★
1835–7150	1829–718	No ID	1.1	0.0	+0.000	0.015	–	–	–	–
1837–7108	1831–711	QSO	2.4	1.5	**+0.115**	0.008	+0.30	0.02	3.2	0.4
1912–8010	1903–802	QSO	1.0	2.7	**−0.059**	0.009	−0.17	0.04	3.1	0.4
1930–6056	1925–610	QSO	1.0	3.3	**−0.087**	0.014	−0.19	*	–	–
1939–6342	1934–638	G (GPS)	5.8	0.0	**+0.029**†	0.005†	−0.91	0.01	1.1	0.4
1940–6908	1935–692	QSO	0.9	1.4	**−0.075**	0.010	−0.45	0.02	1.8	0.2
2009–4849	2005–489	BLC	1.5	5.0	−0.003	0.009	−0.04	0.03	8.4	0.9
2152–7807	2146–783	QSO (GPS)	1.2	0.1	**−0.079**	0.005	+0.12	0.03	1.0	0.1
2243–2544	2240–260	BLC	0.7	4.2	+0.039	0.013	−0.21	0.03	1.2	0.1

Notes for Table 3: ★ steep-spectrum sources with no variability data; † derived from observations of CSS sources; * Spectral index obtained from Parkes Catalogue data (Wright & Otrupeck 1990).

most of the significantly variable sources in the survey are included, and the calibration procedure is consistent across all epochs and sources.

The definition of *WFI* does not take into account the dates of the observations, which are obviously important; a source which varies by 0.1 Jy in one day is much more variable than a source which varies by 0.1 Jy over a year, yet they would have the same *WFI*! The temporal coverage of most of the objects in the ATCA flux monitoring survey is similar, however, and as most of the variability data have been taken from this survey the simplification of temporal independence in the definition of *WFI* has been used.

There are a number of sources for which there are circular polarization measurements but no flux-monitoring data. Several of these are steep-spectrum sources (marked with a '★' in Table 3), for which no significant variability is expected on the time-scale of the monitoring programme. These sources have arbitrarily been assigned $WFI = 1$ per cent, this being similar to the *WFI* measured for the GPS sources PKS 1934−638 and PKS 0823−500. The *WFI* for PMNJ 0229−7847 was estimated using privately collected ATCA flux-monitoring data.

The spectral indices $\alpha_{3-20\,\mathrm{cm}}$ (where $I \propto \nu^{+\alpha}$) were also taken, where possible, from the ATCA flux-monitoring data. If possible, the quoted spectral index was interpolated from the two monitoring epochs closest to the time of the polarization observation. Where monitoring data were not available, or were degraded by structure or confusion, Parkes catalogue (Wright & Otrupcek 1990) data were substituted; these sources are marked with an asterisk in the $\sigma_{\alpha_{3-20\,\mathrm{cm}}}$ column in Table 3.

3.8 Circular polarization monitoring data

Circular polarization variability data from a pilot study are included in this paper. The aim of the pilot study was to determine the approximate time-scales of circular polarization variations in AGN, as a prelude to a possible long-term circular polarization monitoring campaign. As a result of this aim, and the vagaries of the time-allocation process, the observations were not uniformly spaced in time.

Four sources were selected for this pilot study: the BL Lac sources PMNJ 0428−3756 and PMNJ 0538−4405 were selected on account of their high circular polarization and extreme variability, the quasar PMNJ 0229−7847 was chosen because of its very high fractional circular polarization, and the presumably non-variable CSS galaxy PMNJ 0252−7104 was included as a check-source.

The observation and calibration procedures for the circular polarization monitoring observations and the survey observations were similar. The observations were scheduled so as to obtain good parallactic-angle coverage for all sources.

4 RESULTS

The circular polarization survey results are shown in Table 3. The linear and circular polarization per centages are given in the *LP* and *V/I* columns, respectively.

4.1 Circular polarization of intraday variable sources

The intraday variable (IDV) BL Lac source PMNJ 1522−2730 (PKS 1519−273) showed significant variation in both total intensity and polarization during the 10 hours over which it was observed. We were thus unable to image the source, but the high flux density of the source and lack of significant confusion enabled us to measure instead the flux variation with time. The visibilities, combined from all baselines and 30-minute-averaged, are shown in Fig. 2. The quoted error for $\sigma_{V/I}$ for PMNJ 1522−2730 in Table 3 is the average error in each 30-min integration. For the purposes of the statistical analyses described later in this chapter, the circular polarization of PMNJ 1522−2730 is represented by the time-averaged value of $V/I = -0.37$ per cent. The error bars for the PMNJ 1522−2730 data points in Figs 5 and 6 represent the extremes of the circular polarization variations during the day of the observations, not the errors in the measurements. Since the discovery of the IDV circular polarization in this survey, PMNJ 1522−2730 has been the subject of a more detailed study (Macquart et al. 2000).

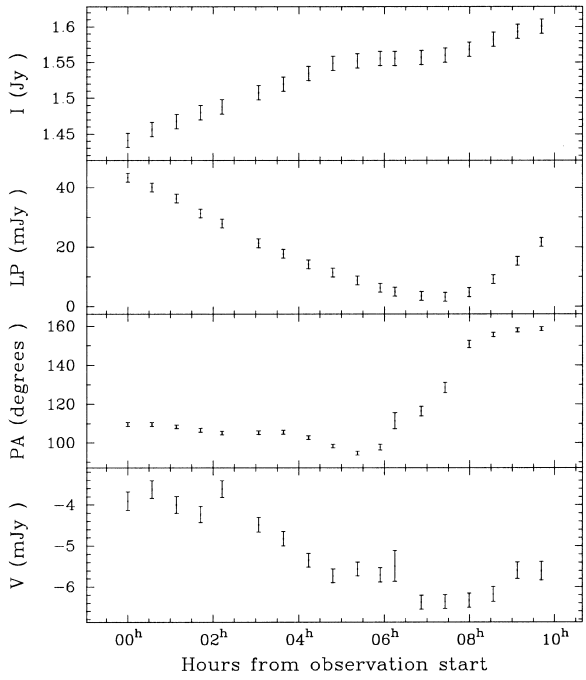

Figure 2. Total-intensity and polarization variations in the IDV BL Lac source PMNJ 1522−2730 (PKS 1519−273), averaged over all baselines. Data points are 30-minute averages.

We note also that the BL Lac source PMNJ 1037−2934 (PKS 1034−293) shows significant variation in linear polarization during the survey observation, and also appears to show variable circular polarization. The calibration is somewhat uncertain for PMNJ 1037−2934, however, and we do not discuss it further here.

4.2 Circular polarization and optical classification

The distributions of magnitude-only fractional circular polarization (as circular polarization can be either positive or negative) for the different optical classes are shown in Fig. 3.

Visual inspection suggests that BL Lac objects show higher circular polarization than quasars, and quasars higher than galaxies. We have conducted statistical tests to investigate whether there really are significant differences between the circular polarization distributions for the optically classified subsamples.

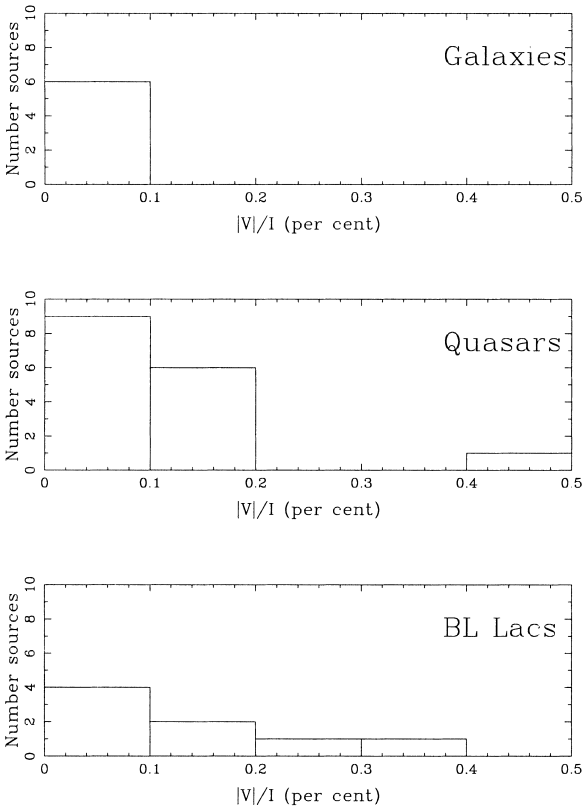

Figure 3. Distributions of fractional circular polarization for the AGN optical classifications.

Table 4. Results of KS tests to compare the circular polarization between the optical classes.

Class 1	Class 2	Smirnov Statistic	Occur by Chance (per cent)
BL Lacs	Galaxies	0.875	0.6
Quasars	Galaxies	0.812	0.5
BL Lacs	Quasars	0.187	98.3

The sensitivity of statistical tests is severely limited, of course, by the small size of the samples.

4.2.1 *Kolmogorov–Smirnov tests*

The one-tailed Kolmogorov–Smirnov two-sample test Conover (1971, hereafter the KS test) gives the probability that one sample is drawn from a distribution which is systematically 'larger' than the distribution from which a second sample is drawn. Thus, for this test it is appropriate to use $m_c = |V|/I$ rather than *V/I*. Each optically selected subsample was tested against the other two, and the results are presented in Table 4; the 'Occur by Chance' column gives the probability that the observed differences in the circular polarization subsamples would occur by chance if they were drawn from the same parent distribution. The results show that Galaxies have systematically lower circular polarization than BL Lacs and quasars, but cannot differentiate between the BL Lac and quasar circular polarization distributions.

Using only the magnitude of the detected circular polarization carries the implicit assumption that the samples are drawn from a distribution with a mean of zero ie. *there is no preferred handedness in the circular polarization of extragalactic sources*. As noted above, a bias could occur if the zero-point of the ATCA circular polarization calibration is in error. As a precaution, the KS tests were repeated with an assumed zero-point such that PKS 1934–638 has $V = 0$, but the conclusions are the same.

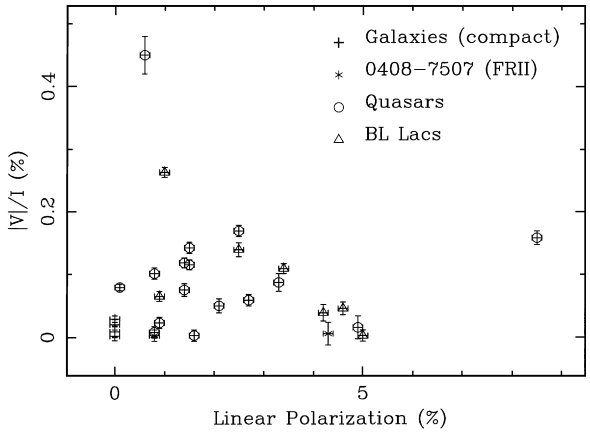

Figure 4. Circular polarization versus linear polarization for the survey sources. The IDV source PMNJ 1522−2730 has been excluded.

4.3 Linear polarization

Perhaps surprisingly, the linear polarization of the survey sources appears to be totally uncorrelated with any of circular polarization, spectral index or variability. A plot of circular polarization versus linear polarization is given in Fig. 4.

The CSS and GPS sources from the sample are obviously distinct, in terms of linear polarization properties, from the blazar sources, as the former all have zero linear polarization. No statistically significant difference was found, however, between the linear polarization of the BL Lac and quasar distributions.

4.4 Circular polarization, spectral indices and total intensity variability

Given the apparent association between blazar objects and circular polarization, we might expect that sources which show higher levels of circular polarization would also show preferentially flat/inverted spectral indices, and higher levels of radio variability. Measures of these two properties are plotted against fractional circular polarization in Figs 5 and 6.

4.4.1 *Spearman rank correlation coefficient tests*

Clearly, sources which show high levels of circular polarization tend to have inverted spectra. Spearman rank correlation coefficient tests, suitable for non-Gaussian parent distributions, were conducted to find the significance of the correlation between Weighted Fluctuation Index (*WFI*) and circular polarization, and between spectral index and circular polarization. The data were found to be correlated at >99 per cent confidence level in both cases.

4.4.2 *Principal component analysis*

Principal Component Analysis (PCA) can be used to identify general factors which influence the variability within a data set

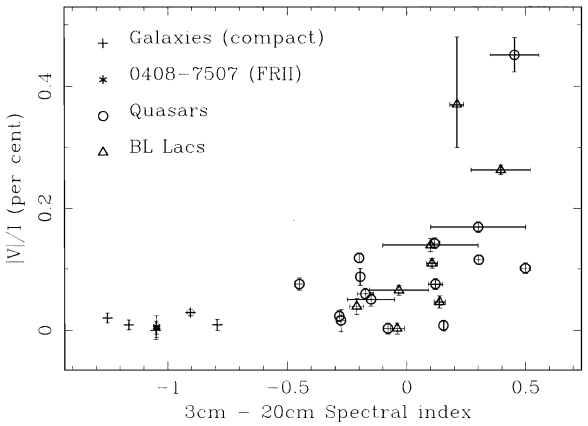

Figure 5. Fractional circular polarization versus 3–20 cm spectral index. The large error bars associated with the PMNJ 1522–2730 data point represent the extremes of the circular polarization variation during the day of the observation.

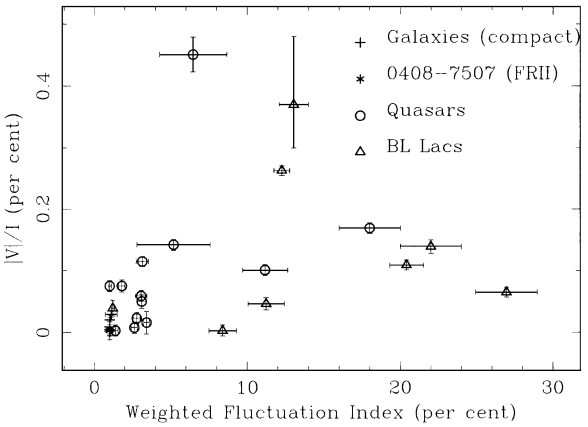

Figure 6. Fractional circular polarization versus Weighted Fluctuation Index. See comments regarding PMNJ 1522–2730 in Fig. 5.

(Jolliffe 1986). The components discovered may or may not have any real physical counterpart, but the aim of PCA is to gain some qualitative understanding of the trends in the data. The non-normalized data used for the PCA are displayed graphically in Fig. 7.

The PCA output is shown in Table 5. The first principal component shows positive coefficients for all variables, and so is a trend for inverted spectrum, variable sources to have higher values of circular polarization. This component can be thought of as a general measure of 'blazarness', related to physical parameters such as source size, activity, the angle between the jet-axis and the line of sight and, for whatever reason, circular polarization.

The second component is probably an artefact; the first principal component has probably taken up all the variability which can be discerned above the natural scatter in the data. No investigation of the significance of this component has been attempted.

4.5 Circular polarization monitoring results

The results from the circular polarization monitoring pilot study are shown graphically in Fig. 8. The sensitivity and reliability of

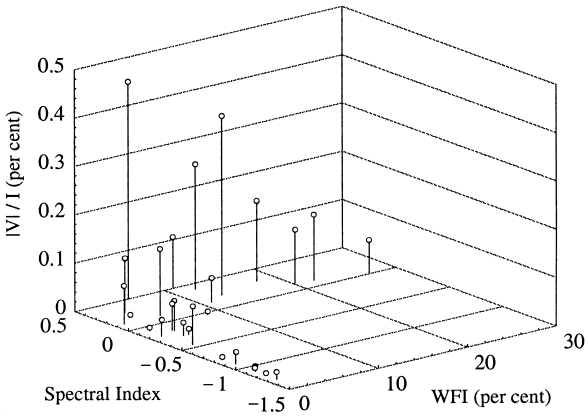

Figure 7. Three-axis plot of unsigned fractional circular polarization versus 3–20 cm spectral index and weighted fluctuation index.

Table 5. Principal Component Analysis results.

Component number	% of total variation	Coefficients m_c (%)	*WFI* (%)	α
1	67.0	+0.571	+0.541	+0.617
2	20.6	+0.617	−0.779	+0.112
3	12.4	+0.541	+0.317	−0.779

the observations are demonstrated by the results for the CSS source PMNJ 0252–7104 (PKS 0252–712), for which there is no significant circular polarization detection or variability over a year, with $\sigma_{V/I} \lesssim 0.01$ per cent.

The pilot study does reveal a few important aspects of circular polarization variability. The detection of rapid changes in circular and linear polarization in PMNJ 0538–4405 (PKS 0537–441) between epochs 829 and 879 suggests that, in some sources at least, the difficulty in interpreting published circular polarization variability data may be complicated by undersampling.

In no case do we detect a sign-change in the circular polarization, so our results are consistent with published results, which suggest that sources have a *preferred handedness* (Komesaroff et al. 1984). The circular polarization in PMNJ 0538–4405 (PKS 0537–441) peaks at $m_c = 0.26$ per cent when the total intensity drops to a minimum, but a year later appears to be circularly unpolarized. This may represent a *V*-quiescent state, or may be a transition stage from left- to right-handed polarization. Further observations of this source would definitely be of interest.

A more detailed analysis is frustrated by the sparsity of the data, and we draw no conclusions regarding the relationship between variations in circular polarization and variations in total intensity or linear polarization.

5 DISCUSSION

The question of the origin and nature of the circular polarization deserves some speculative consideration, although we do not pretend that the data presented here can provide definite answers.

5.1 Circular polarization emission regions

The lack of circular polarization in CSS sources and the

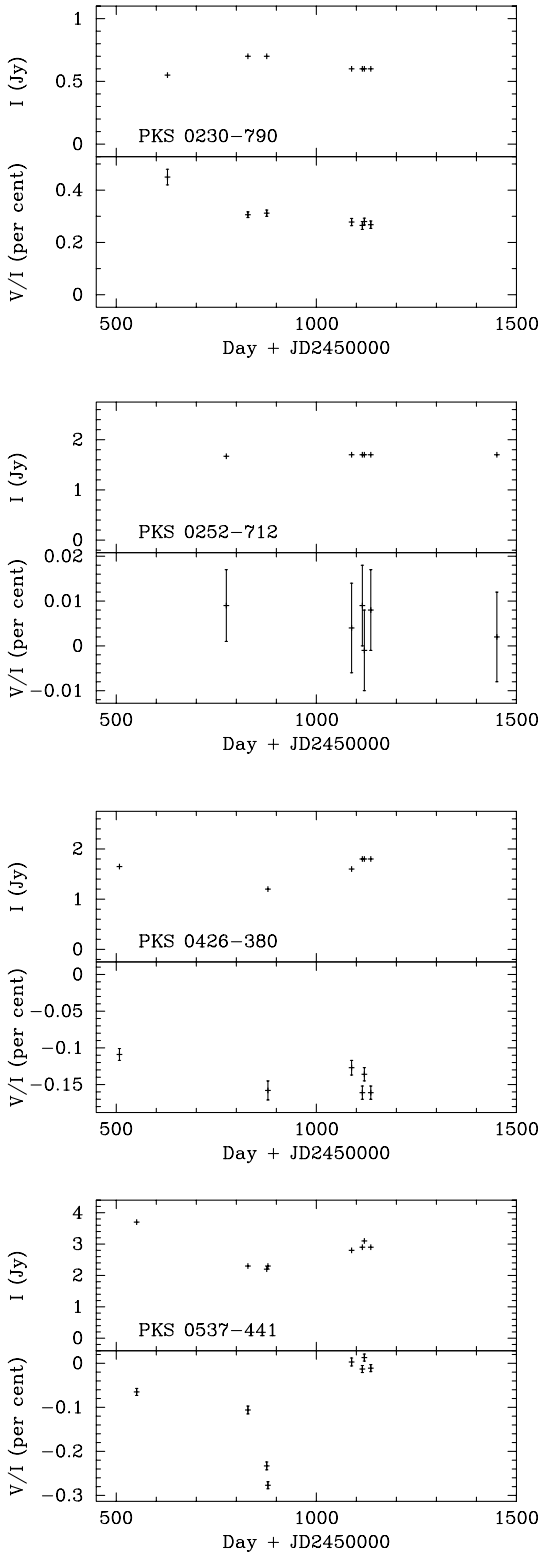

Figure 8. 4800-MHz circular polarization flux-monitoring data. (a) PKS 0230−790; (b) PKS 0252−712; (c) PKS 0426−380; (d) PKS 0537−441.

correlation of circular polarization with blazar characteristics suggests that circular polarization originates in compact components in the AGN core. This conclusion is further strengthened by observations of significant variability in the circular polarization of blazar sources, which indicates that the circular polarization in these sources must be associated with small spatial regions. While these conclusions are not new, they are made here based on data of much higher quality than previously available.

5.2 Is circular polarization intrinsic to synchrotron emission?

First, we note that the theoretically predicted degree of circular polarization from homogeneous synchrotron emission is of order $1/\gamma$, where the Lorentz factor of the emitting electrons is thought to be typically $100 < \gamma < 1000$ (Burbidge, Jones & O'Dell 1974; Jones & O'Dell 1977). In comparison, the linear polarization can be up to 70 per cent. Random inhomogeneities in the field direction and source structure are expected to reduce both linear and circular polarization by a similar amount. For the BL Lac sources and some of the quasars in our survey, however, the ratio of circular-to-linear polarization is obviously much higher than predicted by synchrotron theory. This apparent inconsistency has been termed the *circular polarization excess* by Valtaoja (1984), and is a strong argument against significant intrinsic synchrotron emission.

If the circular polarization is due to intrinsic synchrotron emission, some preferred orientation of the magnetic field is required to account for the excess. The commonly quoted expression for fractional circular polarization for a plasma with a uniform magnetic field from Legg & Westfold (1968) gives $m_c \propto (\sin\theta)^{1/2}\cot\theta$, where θ is the angle of the magnetic field with respect to the line of sight. Even though the divergence of m_c as $\theta \rightarrow 0$ is artificial, this formula does suggest that the ratio of linear-to-circular polarization could be increased if the source was viewed with the magnetic field close to the line of sight. VLBI polarization images indicate that the magnetic fields in BL Lac jets are preferentially *perpendicular* to the jet direction on parsec scales (Gabuzda et al. 1992), however, so it seems unlikely that we are detecting intrinsic circular polarization from the parsec-scale jet in these sources. Wardle et al. (1998) reach the same conclusion from analysis of circular polarization VLBI observations of the core of the BL Lac-like quasar 3C 279.

The situation for the VLBI cores is not so well established. The polarization position angles in the cores of BL Lac objects appear to be randomly oriented with respect to the milliarcsecond-scale structure (Gabuzda et al. 1992). This apparent randomness is presumably due to structural misalignments, orientation effects where the jet is at a small angle to the line of sight, or possibly Faraday rotation (Cawthorne et al. 1993), and so the observed polarization position angle does not represent the true magnetic field orientation at the jet optical surface. Although it seems likely that the observed circular polarization does originate from the jet optical surface, it is impossible to determine the contribution of intrinsic synchrotron emission from the current observations.

5.3 Is circular polarization a propagation effect?

A different possibility is that circular polarization arises during wave propagation in a relativistic plasma. In simple models of homogeneous synchrotron sources, linear-to-circular conversion can theoretically produce circular polarization approaching $m_c \sim$ 10 per cent, albeit for a narrow range of parameters close to the spectral turnover frequency (Jones & O'Dell 1977). This suggests that the conversion mechanism is much more efficient at generating circular polarization than synchrotron emission itself.

The theoretical value of $m_l \sim 70$ per cent for the linear polarization is observed only when the AGN jets are observed with VLBI resolution; the 'integrated' linear polarization of the AGN in our survey is typically $m_l \sim 1$–3 per cent, so the linear-to-circular polarization ratio expected from the circular-repolarization mechanism is broadly consistent with the results presented here.

5.4 Variability of circular polarization

The observation of significant variations in the circular polarization of some BL Lac objects implies that circular polarization is associated with compact regions in these sources. While there are a number of mechanisms which could produce circular polarization variations, the apparent tendency of sources to have a preferred handedness implies some persistent magnetic anisotropy in the region responsible for the circular polarization.

The observation of circular polarization variations in BL Lac sources also has implications for the investigation of the relationship between circular polarization and other source properties. Any tests which use only a single polarization measurement for each source implicitly assume that the polarization is not variable, and that the measured distribution represents different sources having different polarization. The detection of variable circular polarization in the BL Lac sources suggests that at best this is only half the story, and that changes in the polarization for individual sources will also contribute significantly to the observed circular polarization distribution. We cannot rule out the possibility that all blazar sources show comparatively high levels of circular polarization at some epochs.

5.5 Polarization of CSS and GPS radio galaxies

It is also important to question why the CSS and GPS sources in the survey have much lower observed circular polarization than the blazar sources; does the mechanism which produces observable circular polarization in the cores of blazar AGN not operate in the more extended emission region of the radio galaxies?

Given that none of the CSS sources observed in the survey showed any linear polarization, a starting point would be to examine whether the same mechanism is depolarizing both the linear and circular polarization. Possible mechanisms for the depolarization of linear polarization in CSS and GPS sources include (O'Dea 1998): large-scale polarization structure, such that polarization contributions from different regions in the source cancel each other; a locally inhomogeneous magnetic field, which would mean that even fairly small regions in the source would have zero net linear polarization; or internal/external Faraday rotation. Source structure or magnetic field inhomogeneities might be expected to depolarize a source similarly in linear and circular polarization, and may account for the lack of detectable circular polarization in the linearly unpolarized CSS sources in our survey. We note, however, that Faraday rotation in a (presumably 'cold') external plasma will not affect the incident circular polarization. We also note that the only radio galaxy where we have confidently detected circular polarization (albeit indirectly) is the GPS source PKS 1934–638; this is also the only radio galaxy with a turnover frequency close to the observing frequency. We are planning further observations of GPS sources.

5.6 Circular polarization and electron–positron jets

In a recent publication, Wardle et al. (1998) suggest that circular polarization measurements of the quasar 3C 279 imply the existence of substantial 'pair' (electron–positron) plasma in the core emission-region. Their results are based on the implications of a low value of γ_i (the relativistic electron low-energy cut-off) on the jet-plasma composition. For an electron–proton jet, γ_i must be fairly high, or else much more energy would be carried by the jet than is observed to be dissipated. For an e^+e^- jet, a low γ_i is required, or there is not enough energy carried. The same implication follows from the detection of linear polarization in VLBI jets; if the jets are e^-p^+, a high γ_i is required to prevent the jet being Faraday-depolarized.

Wardle et al. (1998) evaluate numerical models for 3C 279; they derive most parameters from their observations, and then explore possible values of γ_i which give the observed linear polarization, circular polarization, and Faraday depth. The circular polarization observations are particularly important, as conversion of linear polarization to circular is highly sensitive to γ_i. Wardle et al. claim they are unable to find a model which fits the observed parameters with $\gamma_i > 20$, thus implying a low γ_i and hence a dominantly e^+e^- jet.

The circular polarization data reported here, while at a much higher precision than the results of Wardle et al. are not suitable for determining the plasma composition because of the limited resolution of the ATCA. Source modelling would require observations at several frequencies from which to estimate the Faraday depth and opacity, and VLBI or comprehensive polarization-monitoring data with which to estimate the source brightness and magnetic fields.

6 CONCLUSIONS

We have detected circular polarization with high precision using the ATCA. A survey of strong, compact AGN has shown the following.

(i) BL Lacs and quasars have stronger circular polarization, on average, than compact radio galaxies.

(ii) The circular polarization of BL Lac sources varies significantly on time-scales ranging from weeks to years, but with no evidence of a sign-change.

(iii) There is a strong correlation between spectral index and circular polarization.

(iv) There is a strong correlation between variability and circular polarization.

(v) Circular polarization has been observed to vary on time-scales of less than a day in at least one intraday variable source.

ACKNOWLEDGMENTS

We thank Mike Kesteven and the engineering staff of the Australia Telescope for their enthusiastic support in overcoming the challenges associated with the measurement of these low levels of circular polarization. We thank Steven Tingay and Edward King for supplying us with the ATCA flux-monitoring data, Niven Tasker, Alan Wright and Oliver Prouton for the use of the CASNAP data base, Jim Lovell for access to unpublished ATCA survey data, Simon Wotherspoon for assistance with the statistical analysis, and John Wardle for his helpful suggestions. DPR acknowledges support of an Australian Postgraduate Award. The Australia Telescope is funded by the Commonwealth of Australia for operation as a National Facility managed by CSIRO. This research has made extensive use of the NASA/IPAC Extragalactic

Data base (NED) which is operated by the Jet Propulsion Laboratory, California Institute of Technology, under contract with the National Aeronautics and Space Administration.

REFERENCES

Alvarez I., Aparici J., May J., Navarrete M., 1993, A&A, 271, 435
Anguita C., Campusano L. E., Torres C., Pedreros M., 1979, AJ, 84, 718
Bergeron J., Kunth D., 1984, MNRAS, 207, 263
Blandford R. D., Königl A., 1979, ApJ, 232, 34
Bolton J. G., Savage A., 1977, Aust. J. Phys. Astrophys. Suppl., 41, 25
Burbidge G. R., Jones T. W., O'Dell S. L., 1974, ApJ, 193, 43
Cawthorne T. V., Wardle J. F. C., Roberts D. H., Gabuzda D. C., 1993, ApJ, 416, 519
Conover W. J., 1971, Practical Nonparametric Statistics. John Wiley & Sons Inc., New York
Conway R. G., Gilbert J. A., Raimond E., Weiler K. W., 1971, MNRAS, 152, 1P
Cristiani S., Koehler B., 1987, A&AS, 68, 339
di Serego Alighieri S., Danziger I. J., Morganti R., Tadhunter C. N., 1994, MNRAS, 269, 998
Duncan R. A., Sproats L. N., 1992, Publ. Astron. Soc. Aust., 10, 16
Ekers R. D., Weiler K. W., van der Hulst J. M., 1975, A&A, 38, 67
Espey B. R., Carswell R. F., Bailey J. A., Smith M. G., Ward M. J., 1989, ApJ, 342, 666
Falomo R., 1996, MNRAS, 283, 241
Falomo R., Maraschi L., Treves A., Tanzi E. G., 1987, ApJ, 318, L39
Falomo R., Scarpa R., Bersanelli M., 1994, ApJS, 93, 125
Fanaroff B. L., Riley J. M., 1974, MNRAS, 167, 31P
Fosbury R. A. E., Bird M. C., Nicholson W., Wall J. V., 1987, MNRAS, 225, 761
Fosbury R. A. E., Morganti R., Wilson W., Ekers R. D., di Serego Alighieri S., Tadhunter C. N., 1998, MNRAS, 296, 701
Frater R. H., Brooks J. W., Whiteoak J. B., 1992, J. Electrical Electron. Eng. Aust., 12, 103
Gabuzda D. C., Cawthorne T. V., Roberts D. H., Wardle J. F. C., 1992, ApJ, 388, 40
Gilbert J. A., Conway R. G., 1970, Nat, 227, 585
Griffith M., 1992, BAAS, 181, 113.05
Hewitt A., Burbidge G., 1993, ApJS, 87, 451
Hunstead R. W., Lasker B. M., Mintz B., Smith M. G., 1971, Aust. J. Phys., 24, 601
Hunstead R. W., Murdoch H. S., Shobbrook R. R., 1978, MNRAS, 185, 149
Jauncey D. L., Wright A. E., Peterson B. A., Condon J. J., 1978, ApJ, 219, L1
Jauncey D. L., J B. M., Wright A. E., Peterson B. A., Savage A., 1984, ApJ, 286, 498
Jauncey D. L., Savage A., Morabito D. D., Preston R. A., Nicolson G. D., Tzioumis A. K., 1989, AJ, 98, 54
Jolliffe I. T., 1986, Principal Component Analysis, Springer Series in Statistics. Springer-Verlag, New York
Jones T. W., O'Dell S. L., 1977, ApJ, 214, 522
Kennett M., Melrose D. B., 1998, Publ. Astron. Soc. Aust., 15, 211
Kesteven M. J., 1995, ATNF Technical Document Series 39.3/056. Australia Telescope National Facility
Koekemoer A., 1996, PhD thesis, Australian National Univ.
Komesaroff M. M., Roberts J. A., Milne D. K., Rayner P. T., Cooke D. J., 1984, MNRAS, 208, 409
Legg M. P. C., Westfold K. C., 1968, ApJ, 154, 499
Lovell J., 1996, PhD thesis, Univ. Tasmania
Macquart J. P., Melrose D. B., 1998, BAAS, 193, 83.01
Macquart J.-P., Kedziora-Chudczer L., Rayner D. P., Jauncey D. L., 2000, ApJ, 538, 623
Melrose D. B., 1971, Ap&SS, 12, 172
Melrose D. B., 1997, J. Plasma Phys., 58, 735
Morris S. L., Ward M. J., 1998, MNRAS, 230, 639
Morton D. C., Savage A., Bolton J. G., 1978, MNRAS, 185, 735
O'Dea C. P., 1998, PASP, 110, 493
Osmer P. S., Porter A. C., Green R. F., 1994, ApJ, 436, 678
Pacholczyk A. G., 1973, MNRAS, 163, 29P
Pacholczyk A. G., Swihart T. L., 1974, ApJ, 192, 591
Peterson B. A., Bolton J. G., 1972, Astrophys. Lett., 10, 105
Reynolds J. E. and the SHEVE team, 1993, in Davis R. J., Booth R. S., eds, Sub-Arcsecond Radio Astronomy. Cambridge Univ. Press, Cambridge, p. 156–159
Reynolds J. E., 1994, ATNF Technical Document Series 39.3/040. Australia Telescope National Facility
Reynolds J. E., 1997, ATCA Calibrator Source Catalogue. ftp://ftp.atnf.csiro.au/pub/atnfdocs/guides/at.cat
Roberts J. A., Komesaroff M. M., 1965, Icarus, 4, 127
Roberts J. A., Roger R. S., Ribes J. C., Cooke D. J., Murray J. D., Cooper B. F. C., Biraud F., 1975, Aust. J. Phys., 28, 325
Romerno G. E., Benaglia P., Combi J. A., 1995, A&A, 301, 33
Ryle M., Brodie A. C., 1981, MNRAS, 196, 567
Sault R. J., Killeen N. E. B., Kesteven M. J., 1991, ATNF Technical Document Series 39.301, Australia Telescope National Facility
Sault R. J., Teuben P. J., Wright M. C. H., 1995, in Shaw R., Payne H. E., Hayes J. J. E., eds, Astronomical Data Analysis Software and Systems IV, ASP Conf. Ser., Vol. 77. Astron. Soc. Pac., San Francisco, p. 433
Savage A., Wright A. E., 1981, MNRAS, 196, 927
Seaquist E. R., Gregory P. C., Clarke T. R., 1974, AJ, 79, 918
Seielstad G. A., Berge G. L., 1975, AJ, 80, 271
Stickel M., Kühr H., 1996, A&AS, 115, 11
Stickel M., Fried J. W., Kühr H., 1989, A&AS, 80, 103
Stickel M., Fried J. W., Kühr H., 1993, A&AS, 98, 393
Stickel M., Meisenheimer K., Kühr H., 1994, A&AS, 105, 211
Strittmatter P. A., Serkowski K., Carswell R., Stein W. A., Merrill K. M., Burbidge E. M., 1972, ApJ, 175, L7
Tadhunter C. N., Morganti R., di Serego Alighieri S, Fosbury R. A. E., Danziger I. J., 1993, MNRAS, 263, 999
Tornikoski M. et al., 1999, AJ, 118, 1161
Urry C. M., Padovani P., 1995, PASP, 107, 803
Valtaoja E., 1984, Ap&SS, 100, 227
Véron P., Véron-Cetty M. P., Djorgovski S., Magain P., Meylan G., Surdej J., 1990, A&AS, 86, 543
Wall J. V., Cannon R. D., 1973, Aust. J. Phys. Astrophys. Suppl., 31, 1
Wall J. V., Pettini M., Danziger I. J., Warwick R. S., Wamsteker W., 1986, MNRAS, 219, 23P
Wardle J. F. C., Homan D. C., Ojha R., Roberts D. H., 1998, Nat, 395, 457
Weiler K. W., De Pater I., 1983, ApJS, 52, 293
Weiler K. W., Wilson A. S., 1977, A&A, 58, 17
Wilkes B. J., 1986, MNRAS, 218, 331
Wilkes B. J., Wright A. E., Jauncey D. L., Peterson B. A., 1983, Proc. Astron. Soc. Aust., 5, 2
Wright A. E., Otrupcek R., 1990, Parkes Catalogue 1990. Australia Telescope National Facility
Wright A. E. et al., 1997, Accurate Positions, Fluxes and Structure for 6603 Southern Radio Sources. http://www.parkes.atnf.csiro.au/databases/surveys/pmn/casouth.pdf

This paper has been typeset from a TEX/LATEX file prepared by the author.